11th World Congress on Computational Mechanics (WCCM XI)
5th European Conference on Computational Mechanics (ECCM V)
6th European Conference on Computational Fluid Dynamics (ECFD VI)
E. Oñate, J. Oliver and A. Huerta (Eds)

RBF-BASED MESHLESS APPROACHES FOR FREQUENCY-DOMAIN ANALYSIS OF HEAT CONDUCTION PROBLEMS

LUÍS M.C. GODINHO* AND DANIEL DIAS-DA-COSTA†

* CICC, Dept. Civil Engineering, University of Coimbra, 3030-788 Coimbra, Portugal,
email:lgodinho@dec.uc.pt, http://www.uc.pt/fctuc/dec

† School of Civil Engineering, The University of Sydney, NSW2006, Australia;
INESCC, University of Coimbra, and Dept. Civil Engineering, University of Coimbra, Portugal,
email: daniel.diasdacosta@sydney.edu.au

Key Words: *Heat conduction, frequency domain, radial basis functions, meshless.*

Abstract. A variety of numerical methods can be applied to study heat conduction problems in solid media. Typical approaches are based on FEM or BEM, although meshfree methods can already be found in the literature, formulated in time-domain and transformed-domain. In this work, we address the application of a RBF interpolation meshless formulation in the frequency domain in transient heat conduction problems. The selected media can be homogeneous or with spatially varying thermal properties (such as in FGMs).

1 INTRODUCTION

Transient heat conduction problems appear in numerous practical situations, such as in the simulation of building heat losses and thermal bridges. Classical computational approaches are based on FEM or BEM, and more recently on meshfree methods, formulated in time-domain and transformed-domain. A different strategy was recently introduced by applying the Fourier transform directly to the governing differential equation and obtaining the solution for each frequency. The corresponding time-domain solution is then derived using the inverse Fourier transformation. This procedure avoids the accuracy drawbacks of the transformed domain approaches and was shown to be effective with BEM [1,2] and the Method of Fundamental Solutions [1]. The drawback is the fact of the existing implementations being constrained to simpler settings for which there are known fundamental solutions. Aiming at introducing a general approach based on the Fourier transformation, the authors herein propose a comprehensive meshless local Petrov Galerking (MLPG) framework. The Heaviside step function is adopted as the test function to avoid domain integrals in the weak-form of the Partial Differential Equation (PDE), leading to a MLPG(5) class method [4]. Radial Basis Functions (RBFs) are selected for the interpolation function [3,4] because they are computationally more efficient over the MLS approach and satisfy the delta function property [6,7].

Different RBFs are available in the literature (e.g. thin plate spline, Multiquadratic (MQ) and Wendland type RBFs), some of which dependent on a free (shape) parameter [7]. Since the

choice of this parameter is not trivial and may influence the accuracy of the computed results, this issue is also addressed in the manuscript.

2 GOVERNING EQUATIONS

There are many situations where the thermal conductivity values can depend on the spatial coordinates (e.g. functionally graded materials – FGMs). In this case, the time-domain governing equation can be written in 2D as:

$$\nabla \cdot \left(k(\mathbf{x}) \nabla T(\mathbf{x},t) \right) = \rho c(\mathbf{x}) \frac{\partial T(\mathbf{x},t)}{\partial t} \ , \tag{1}$$

where $T(\mathbf{x},t)$ is the temperature at domain point $\mathbf{x}$, and k, c and ρ are the thermal conductivity, specific heat and density, respectively.
The Fourier transform can be applied to equation (1) for shifting the problem to the frequency domain, leading to the following frequency-dependent equation:

$$\nabla \cdot \left(k(\mathbf{x}) \nabla \hat{T}(\mathbf{x},\omega) \right) - \mathrm{i}\rho c(\mathbf{x}) \omega \hat{T}(\mathbf{x},\omega) = -\rho c(\mathbf{x}) T_0(\mathbf{x}) \ , \tag{2}$$

where $\hat{T}(\mathbf{x},\omega)$ is the frequency-transformed temperature and T_0 is the initial temperature distribution.

3 FORMULATION OF THE NUMERICAL METHOD

A set of interpolating nodes is scattered throughout domain and boundary. The weak form of the governing equation around each node i is given by [4]:

$$\int_{\Omega_i} \nabla \cdot \left(k(\mathbf{x}) \nabla \hat{T}(\mathbf{x},\omega) \right) v \, d\Omega - \int_{\Omega_i} \mathrm{i}\rho c(\mathbf{x}) \omega \hat{T}(\mathbf{x},\omega) v \, d\Omega = \int_{\Omega_i} -\rho c(\mathbf{x}) T_0(\mathbf{x}) v \, d\Omega \ , \tag{3}$$

where Ω_i is the integration subdomain for node i.

Taking the Heaviside step function as the test function v, which has a unit value inside Ω_i and zero outside, the divergence theorem can be applied to the first integral of equation (3) and the following form can be derived:

$$\int_{\Gamma_{si} \cup \Gamma_{st}} k(\mathbf{x}) \nabla \hat{T}(\mathbf{x},\omega) . \mathbf{n} \, d\Gamma - \int_{\Omega_i} \mathrm{i}\rho c(\mathbf{x}) \omega \hat{T}(\mathbf{x},\omega) v \, d\Omega = \int_{\Omega_i} -\rho c(\mathbf{x}) T_0(\mathbf{x}) v \, d\Omega + \int_{\Gamma_{sf}} \overline{q}(\omega) \, d\Gamma \tag{4}$$

in which Γ_s is the boundary of subdomain Ω_i around the node, decomposed in Γ_{si} (internal boundary), Γ_{st} (boundary with essential conditions) and Γ_{sf} (boundary with heat flow); $\hat{T}$ is the Fourier transform of the temperature and $\overline{q}$ is the imposed heat flow with respect to the normal direction of the boundary ($\mathbf{n}$). A schematic representation of the local boundaries is illustrated in Figure 1.

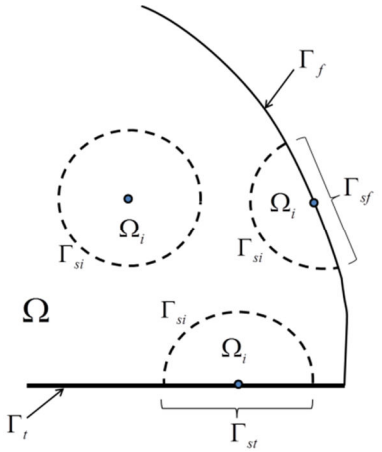

Figure 1: Illustrative representation of a portion of the MLPG domain of analysis, identifying the different local boundaries.

The solution of the PDE is approximated by a set of shape functions that are built by incorporating polynomial terms of the first order. The temperature at a point $\mathbf{x}$ can be defined using a surrounding interpolation domain, with M different nodes, as:

$$\hat{T}(\mathbf{x}) = \sum_{j=1}^{M} R^j(\mathbf{x}) \times B^j + \sum_{j=1}^{NP} P^j(\mathbf{x}) \times C^j \ , \tag{5}$$

with the following constraints:

$$\sum_{j=1}^{M} P^i(\mathbf{x}^j) \times B^j = 0, \text{ for } i = 1..NP \, , \tag{6}$$

where R^j is the interpolation function, B^j and C^j are nodal amplitudes, NP equals 3 when the polynomial terms are of first order and, in this case, P^j is the j^{th} element from $\mathbf{P}(x, y) = [1 \ x \ y]$.

In the present work, different RBFs are tested as interpolation functions:

$$R^j(\mathbf{x}) = r^2 \log(r) \text{ (thin plate spline RBF),} \tag{7}$$

$$R^j(\mathbf{x}) = \sqrt{r^2 + c^2} \text{ (MQ RBF),} \tag{8}$$

$$R^j(\mathbf{x}) = \left(1 - \frac{r}{r_0}\right)_+^4 \left(4\frac{r}{r_0} + 1\right) \text{ (Wendland's compact support RBF of order 2),} \tag{9}$$

where 'c' is a shape parameter, r_0 is the radius of the support domain and $r = \left\| \mathbf{x} - \mathbf{x}^j \right\|$ in all cases.

Writing equations (5) and (6) for a set of M nodes ($\mathbf{x}^1$ to $\mathbf{x}^M$) within a local interpolation domain, the following system of equations can be defined:

$$\hat{\mathbf{T}} = \mathbf{R}_0 \mathbf{Q} \Leftrightarrow \mathbf{Q} = \mathbf{R}_0^{-1} \hat{\mathbf{T}} \tag{10}$$

where $\mathbf{R}_0$ is a matrix given by:

$$\mathbf{R}_0 = \begin{bmatrix} R^1(\mathbf{x}^1) & \cdots & R^M(\mathbf{x}^1) & P^1(\mathbf{x}^1) & \cdots & P^M(\mathbf{x}^1) \\ \vdots & \ddots & \vdots & \vdots & \ddots & \vdots \\ R^1(\mathbf{x}^M) & \cdots & R^M(\mathbf{x}^M) & P^1(\mathbf{x}^M) & \cdots & P^M(\mathbf{x}^M) \\ P^1(\mathbf{x}^1) & \cdots & P^1(\mathbf{x}^M) & 0 & 0 & 0 \\ \vdots & \ddots & \vdots & 0 & 0 & 0 \\ P^M(\mathbf{x}^1) & \cdots & P^M(\mathbf{x}^M) & 0 & 0 & 0 \end{bmatrix} \tag{11}$$

and $\hat{\mathbf{T}}$ is the vector containing the Fourier transformed temperatures at the nodal points of the interpolation domain and $\mathbf{Q} = [B^1 \ldots B^M \;\; C^1 \ldots C^{NP}]^T$.

The Fourier transformed temperature at a generic point $\mathbf{x}$, not necessarily coinciding with a node, can now be written as:

$$\hat{T}(\mathbf{x}) = \mathbf{R}^T(\mathbf{x}) \mathbf{R}_0^{-1} \hat{\mathbf{T}} = \boldsymbol{\Phi}(\mathbf{x}) \hat{\mathbf{T}}, \tag{12}$$

where $\boldsymbol{\Phi}(\mathbf{x}) = [\phi^1(\mathbf{x}) \;\; \ldots \;\; \phi^M(\mathbf{x})]$ are the nodal shape functions and $\mathbf{R} = [R^1(\mathbf{x}) \ldots R^M(\mathbf{x}) \;\; P^1(\mathbf{x}) \ldots P^{NP}(\mathbf{x})]^T$ is the vector containing the values of the RBFs and polynomial functions at point $\mathbf{x}$. It should be noted that the constructed shape functions in equation (12) possess the Kronecker's delta property.

4 PERFORMANCE OF THE METHOD

4.1 Homogeneous medium

The numerical approach is firstly applied to a homogeneous medium with circular shape and unit radius for assessing the accuracy and convergence. The domain has a density of 2500 kg/m^3, a conductivity of 1.4 W/m/ºK and a specific heat of 840 J/kg/ºK. A heat source is located at x=-0.75 m and y=0.0 m (see Figure 2a). The effect of this source in the frequency domain can be accounted using the following solution:

$$\hat{Ts}(\mathbf{x}, \mathbf{x}_s, \omega) = \frac{-\mathrm{i}}{4k} H_0^{(2)}\left(\lambda \left\| \mathbf{x} - \mathbf{x}_s \right\|\right), \tag{13}$$

where $\mathbf{x}_s$ is the position of the source and $H_0^{(2)}$ is the Hankel function of the second kind and order '0'.
The latter function corresponds to the fundamental solution of the homogeneous PDE obtained from equation (2) when $T_0(\mathbf{x}) = 0$.

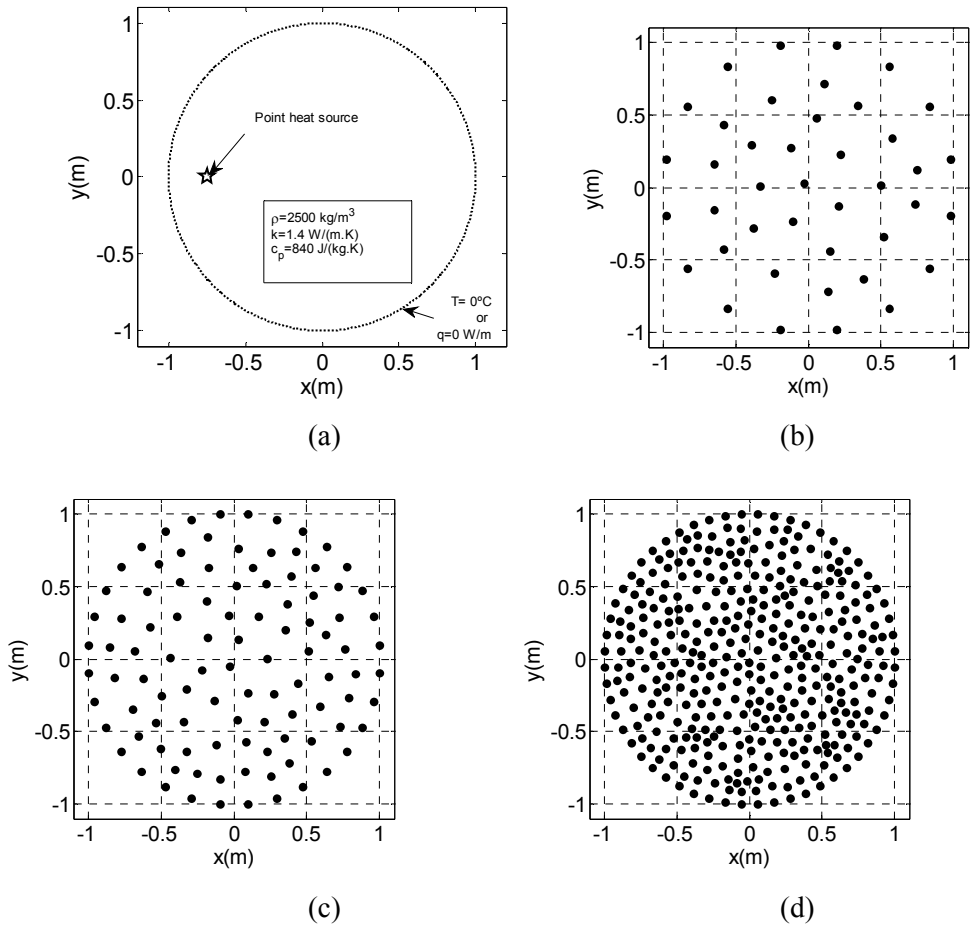

Figure 2:: (a) sketch of the geometry; and different nodal distributions with: (b) h=0.4 m; (c) h=0.25 m; and (d) h=0.125 m.

The three type of RBFs shown in equations (7)-(9) were applied in the analysis of this problem, assuming that the support domain for the Wendland's RBF has the same radius as the interpolation domain at the node. Different values have been tested concerning the free parameter for the MQ RBF with the objective of associating the optimal values with the average spacing between nodal points (h), i.e. $c = L.h$. The selected point distributions are and corresponding spacing are shown in Figures 3b-d. The L2 error norm was computed in all examples using the known solution.

Figure 3 shows the computed error (considering nodal temperature values) for the MQ RBF and varying values of L, when the average spacing between nodal points is h=0.25 m (see Figure 2c). Two frequencies were analysed ($f = 1\times10^{-9}$ Hz and $f = 1\times10^{-5}$ Hz) with two

different boundary conditions, i.e., null temperatures (Figure 3a) and null fluxes (Figure 3b). The obtained results identify an improvement in the response for increasing values of $L = c / h$. However, in Figure 3b, a minimum occurs for $L = 8$. This value is somewhat higher than the one reported in [3], indicating that the typical values observed in elasticity can be different in this type of problems.

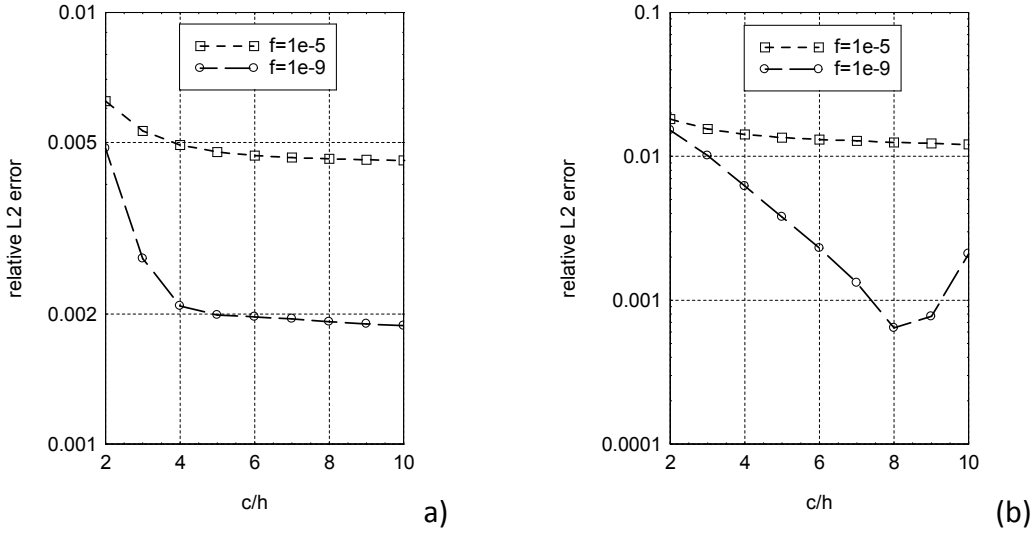

Figure 3: Relative L2 error as a function of the free parameter of the MQ RBF for a system with: (a) null boundary temperature; and (b) null flux boundary conditions.

The convergence of the response is represented in Figure 4 for the different RBFs, considering the same frequencies and boundary conditions.

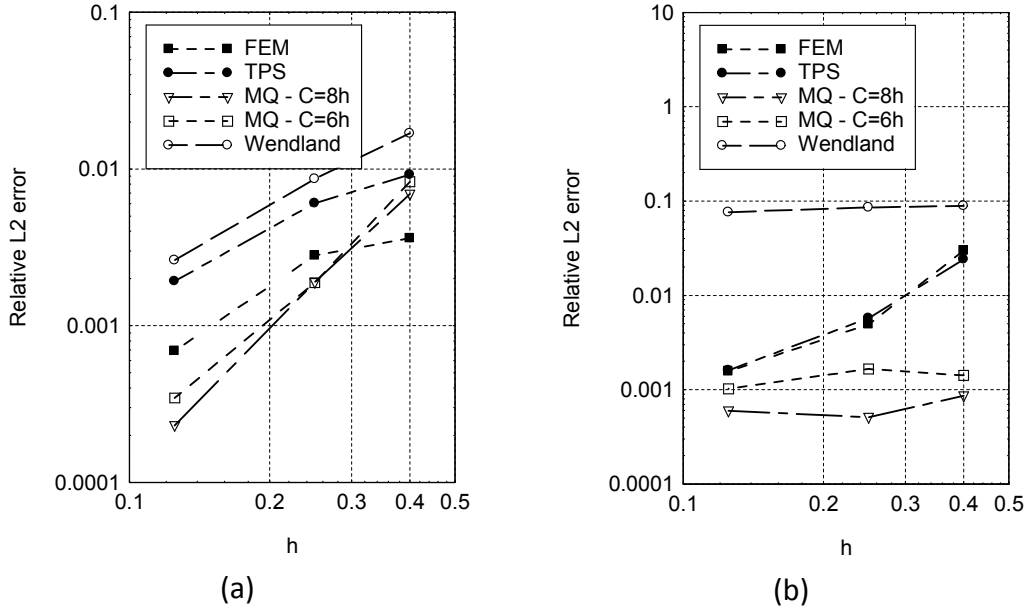

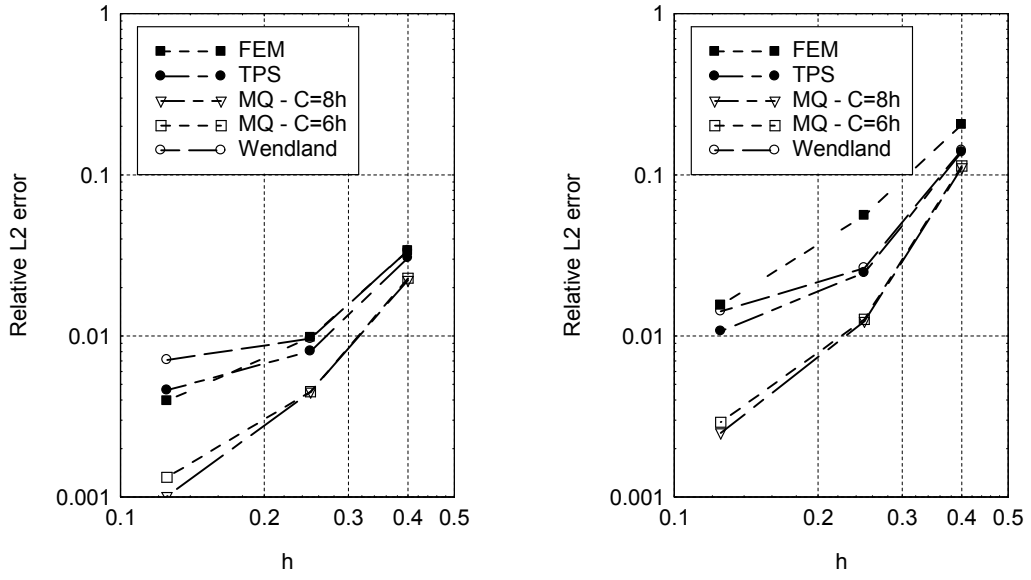

(c) (d)

Figure 4: Relative L2 error for different choices of RBFs. On the left, null boundary temperature: on the right, null flux boundary conditions. (a) and (b) correspond to results for $f = 1\times10^{-9}$ Hz, whereas (c) and (d) correspond to $f = 1\times10^{-5}$ Hz.

Convergence is observed in all tested RBFs and for the MQ with two different shape parameter values, except for the lower frequency with the MQ RBF. Although the convergence is not evident in this case, the computed results show an error smaller than 0.001. Among all RBFs, the Wendland's compact support RBF seems to provide less accurate results, whereas the MQ RBF seems to provide the best overall accuracy in the calculation. The TPS RBF presents an intermediate accuracy performance, which is very close to the finite element method (also represented in the plots). Both the TPS and the MQ RBF are valid choices to build the MLPG shape functions, with better accuracy given by the MQ. In the latter case, the definition of a shape parameter can be a limitation since it requires a prior knowledge of the problem.

4.2 Medium with variable properties

This sub-section addresses an example with a graded material. In this case, a simple rectangular geometry is chosen with 1.0 m x 0.4 m and variable thermal conductivity is enforced along the y-axis. A total of 1137 nodes are randomly positioned throughout the domain and boundary of the problem (Figure 5a), and the temperature variation shown in Figure 5b is applied as boundary condition for x=0.0 m. The material has a density of 2500 kg/m^3 and a specific heat of 840 J/kg/ºK, while its conductivity is given by $k(\mathbf{x}) = 1.4\,(1+2y)$ W / m/º K. As in the previous example, a reference solution has been obtained using a time-domain FEM model.

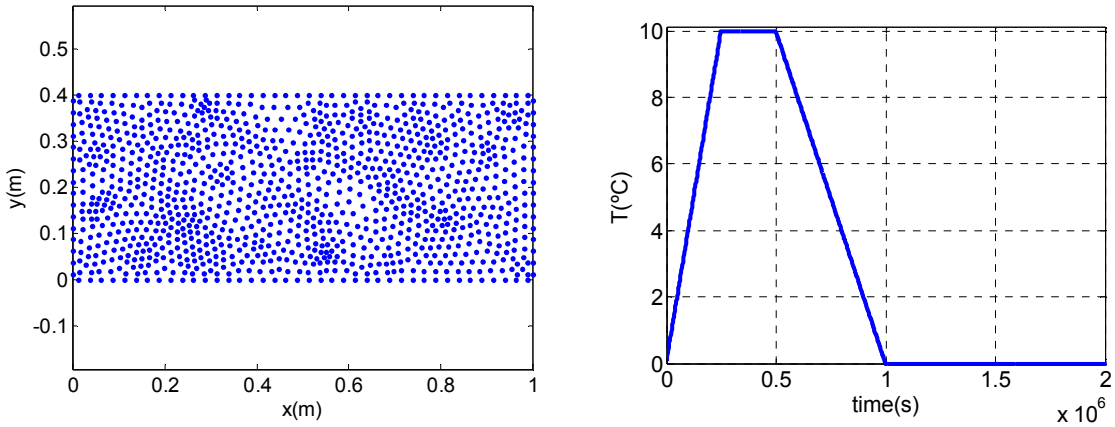

Figure 5: a) Point distribution; b) Temperature variation imposed along the left boundary.

Figure 6 illustrates the temperature evolution registered at a single receiver located at x=0.866 m and y=0.196 m. Two curves are displayed corresponding to both MLPG(5) and time-domain FEM models. The two formulations provide similar results with the temperature varying smoothly as time progresses. This highlights the possibility of using the new approach as an alternative to more common methods available for this type of heterogeneous medium.

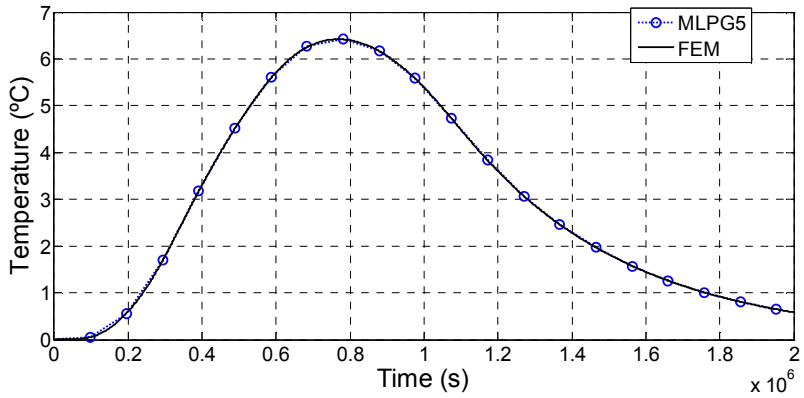

Figure 6: Temperature evolution at an internal point defined by x=0.866 m and y=0.196 m.

5 FINAL REMARKS

This paper presented and discussed the application of a meshless RBF based method for the analysis of transient heat diffusion problems, based on a transformed (frequency) domain. The method was implemented and validated against reference solutions. In the case of a homogenous medium, the proposed MLPG approach provided better convergence rates and accuracy over the traditional FEM method. The proposed approach also showed good

performance in the case of a heterogeneous medium, significantly widening the range of problems that can be efficiently dealt with.

ACKNOWLDEGMENT

This work has been framed under the Initiative Energy for Sustainability of the University of Coimbra and supported by the Energy and Mobility for Sustainable Regions - EMSURE - Project (CENTRO-07-0224-FEDER-002004).

REFERENCES

[1] Godinho, L.; Tadeu, A.; Simões, N. Study of transient heat conduction in 2.5D domains using the Boundary Element Method. *Eng. Anal. Bound. Elmts.* (2004) **28**(6): 593-606.

[2] Godinho, L.; Tadeu, A.; Simões, N. Accuracy of the MFS and BEM on the analysis of acoustic wave propagation and heat conduction problems. In Sladek, J., & Sladek, V. (editors): *Advances in Meshless Methods* (2006), Tech Science Press, Encino, California, pp. 177-198.

[3] Xiao, J.R.; McCarthy, M.A. A local Heaviside weighted meshless method for two-dimensional solids using radial basis functions, *Computational Mechanics* (2003), **31**: 301–315.

[4] Atluri, S. N. *The Meshless Local Petrov-Galerkin (MLPG) Method*. Tech. Science Press (2004).

[5] Liu, G.R.; Gu, Y.T. A point interpolation method for two-dimensional solids, *International Journal for Numerical Methods in Engineering* (2001), **50**(4): 937-951.

[6] Shibahara, M.; Atluri, S.N. The meshless local Petrov-Galerkin method for the analysis of heat conduction due to a moving heat source, in welding. *International Journal of Thermal Sciences* (2011) **50**(6): 984-992.

[7] Cheng, A.H.-D. Multiquadric and its shape parameter - A numerical investigation of error estimate, condition number, and round-off error by arbitrary precision computation. *Eng. Anal. Bound. Elmts.* (2012) **36**: 220-239.